

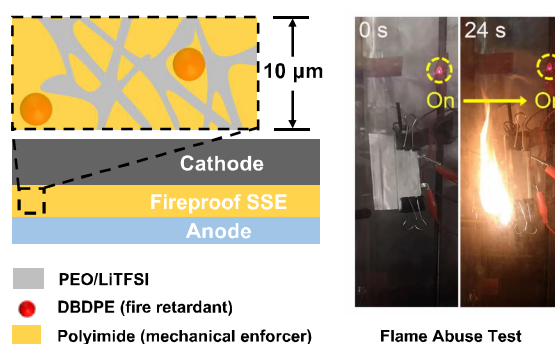
A Fireproof, Lightweight, Polymer–Polymer Solid-State Electrolyte for Safe Lithium Batteries

Yi Cui,[#] Jiayu Wan,[#] Yusheng Ye,[#] Kai Liu, Lien-Yang Chou, and Yi Cui*

ABSTRACT: Safety issues in lithium-ion batteries have raised serious concerns due to their ubiquitous utilization and close contact with the human body. Replacing flammable liquid electrolytes, solid-state electrolytes (SSEs) is thought to address this issue as well as provide unmatched energy densities in Li-based batteries. However, among the most intensively studied SSEs, polymeric solid electrolyte and polymer/ceramic composites are usually flammable, leaving the safety issue unattended. Here, we report the first design of a fireproof, ultralightweight polymer–polymer SSE. The SSE is composed of a porous mechanic enforcer (polyimide, PI), a fire-retardant additive (deca-bromodiphenyl ethane, DBDPE), and an ionic conductive polymer electrolyte (poly(ethylene oxide)/lithium bis-(trifluoromethanesulfonyl)imide). The whole SSE is made from organic materials, with a thin, tunable thickness (10–25 μm), which endorse the energy density comparable to conventional separator/liquid electrolytes. The PI/DBDPE film is thermally stable, nonflammable, and mechanically strong, preventing Li–Li symmetrical cells from short-circuiting after more than 300 h of cycling. $\text{LiFePO}_4/\text{Li}$ half cells with our SSE show a high rate performance (131 mAh g^{-1} at 1 C) as well as cycling performance (300 cycles at C/2 rate) at 60 $^\circ\text{C}$. Most intriguingly, pouch cells made with our polymer–polymer SSE still functioned well even under flame abuse tests.

KEYWORDS: solid-state electrolytes, Li-based batteries, fireproof, polymer–polymer composite, lightweight

Lithium-ion batteries (LIBs) are considered as dominant energy storage devices^{1–4} and ubiquitously applied in modern society from portable electronics to grid-scale storage.^{5–8} In pursuit of LIBs with a higher energy density, a metallic Li anode with high capacity and high voltage cathodes have been intensively studied.^{9,10} However, the increasing demand for energy/power density of LIBs arouses serious safety concerns.^{11,12} Uncontrollable dendritic Li plating triggered at a high current density and accumulated with cycling can penetrate through the separator, leading to intense heat release via an internal short circuit and a potential explosion hazard.^{13,14} There have been a variety of strategies to enhance liquid electrolyte-based battery safety,¹⁵ including ceramic particles coating onto separators,¹⁶ fire retardants in electrolytes,¹⁷ half-short detection,¹⁸ an internal thermal switch,¹⁹ and fire retardant encapsulation by a polymer.²⁰ Replacing soft, flammable separator/liquid electrolytes, solid-state electrolytes (SSEs) could ideally suppress the dendritic Li formation, thus promising the safe operation of LIBs.^{21–23} Commonly studied SSEs can be summarized in three categories: inorganic (ceramic/glass) solid electrolytes, solid polymer electrolytes (SPEs), and their hybrids.^{24–28} The inorganic solid electrolytes have attracted great attention due to the highest ionic conductivity among all types of SSEs. Kato et al. reported superionic lithium conductors with an exceptionally high



conductivity (25 mS cm^{-1} for $\text{Li}_{9.54}\text{Si}_{1.74}\text{P}_{1.44}\text{S}_{11.7}\text{Cl}_{0.3}$), even exceeding that of liquid electrolytes.²⁹ However, air instability, brittleness, large interfacial impedance, and the fact that Li still penetrates inorganic SSEs after critical current density hinders the use of these SSEs in Li-ion batteries.^{30–32} Han et al. discovered that an intrinsic high electronic conductivity in certain inorganic SSEs, especially at grain boundaries, led to hazardous direct Li deposition inside of SSEs.³⁰ In addition, the energy density of batteries with these SSEs is significantly lowered due to the high density and large thickness of inorganic electrolytes.²⁷

SPEs are mainly composed of solid polymers and Li salts, where the solid mixtures serve as Li-ion conductors.^{33–35} Poly(ethylene oxide) (PEO)/Li salts is the most-widely studied polymer system due to its flexibility, low cost, lightweight property, and high Li-ion conductivity among SPEs.^{36,41} However, the intrinsic softness of this polymer system makes it unable to suppress the Li dendrite

conductivity (25 mS cm^{-1} for $\text{Li}_{9.54}\text{Si}_{1.74}\text{P}_{1.44}\text{S}_{11.7}\text{Cl}_{0.3}$), even exceeding that of liquid electrolytes.²⁹ However, air instability, brittleness, large interfacial impedance, and the fact that Li still penetrates inorganic SSEs after critical current density hinders the use of these SSEs in Li-ion batteries.^{30–32} Han et al. discovered that an intrinsic high electronic conductivity in certain inorganic SSEs, especially at grain boundaries, led to hazardous direct Li deposition inside of SSEs.³⁰ In addition, the energy density of batteries with these SSEs is significantly lowered due to the high density and large thickness of inorganic electrolytes.²⁷

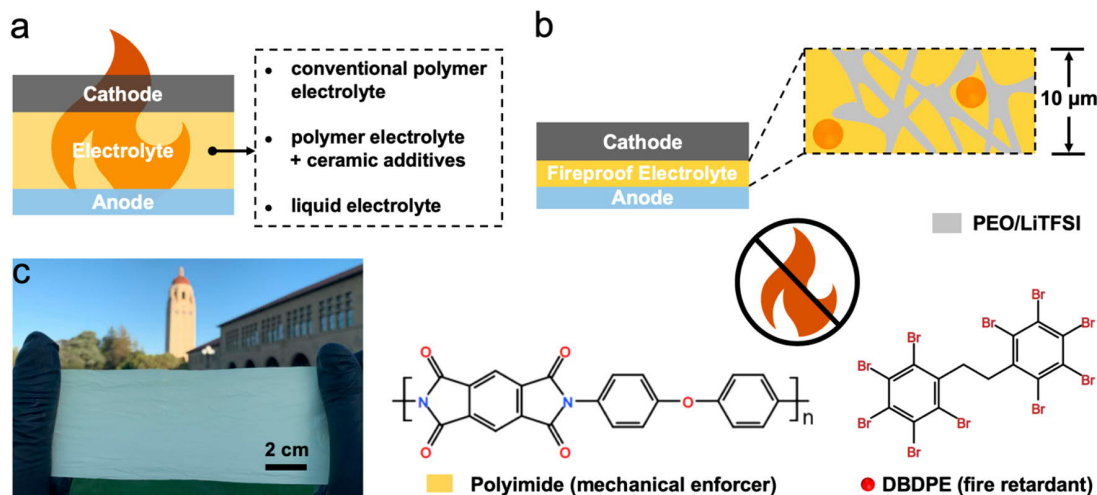


Figure 1. (a) Conventional lithium-based batteries based on liquid and solid polymer-based electrolytes, which are still flammable. (b) Design principles of the fireproof and lightweight polymer–polymer solid-state electrolyte. (c) Photo image of a porous PI/DBDPE film.

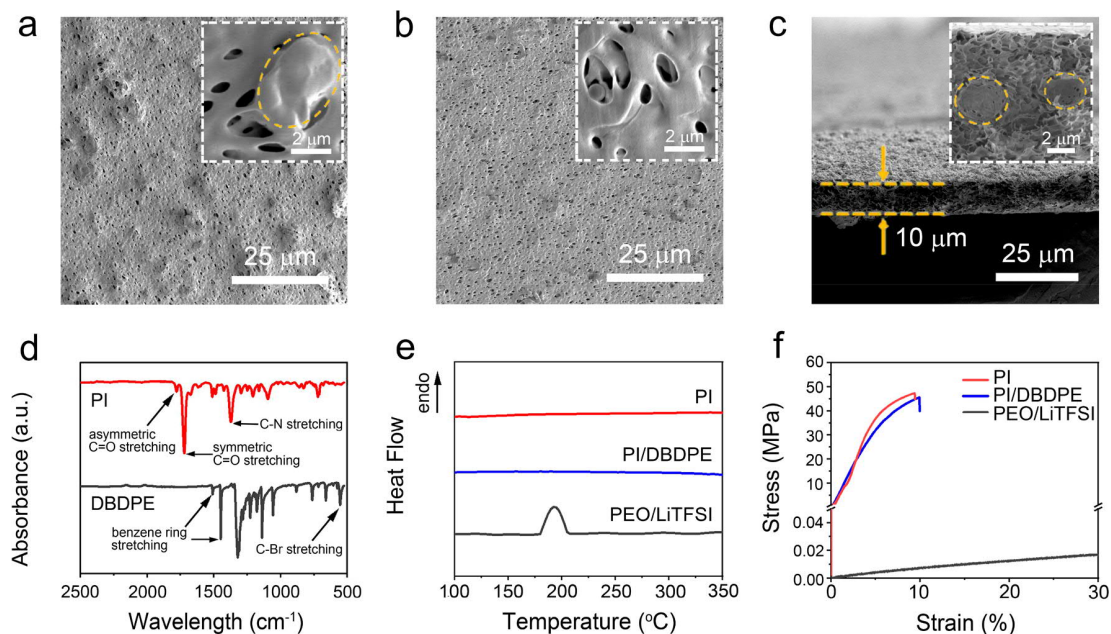


Figure 2. (a) SEM image of the PI/DBDPE film’s surface morphology facing air in the doctor blading process (inset shows a typical magnified SEM image of panel a). (b) SEM image of the PI/DBDPE film’s surface morphology facing glass in the doctor blading process (inset shows a typical magnified SEM image of panel b). (c) Cross-section SEM of a typical PI/DBDPE film showing the thickness of PI/DBDPE film (inset shows a typical magnified SEM image of panel c). Orange dashed circles represent DBDPE particles. (d) FTIR spectra of the PI film and DBDPE particles. (e) The DSC spectra of the porous PI/DBDPE film, porous PI film, and PEO/LiTFSI film. (f) Stress–strain curve of the porous PI/DBDPE film, porous PI film, and PEO/LiTFSI film.

propagation, which restricts its application in LIBs.^{37,38} To circumvent this problem, strategies, such as reinforcing with nanoparticles,^{39,40} cross-linking,^{41,42} and applying with a robust host,^{43–45} were used. Despite their success, these composite polymeric SSEs are still flammable (Figure 1a). Here we investigated the flammability of traditional nanocomposite SSEs. Both PEO/LiTFSI/30 wt % LLZO (Figure S1a and Video S1) and PEO/LiTFSI/30 wt % Al₂O₃ (Figure S1b and Video S2) can still catch fire easily, leaving the original battery safety concern unaddressed.

In this work, we propose the design of a fireproof and ultralightweight SSE with an excellent electrochemical

performance for lithium batteries. The design principles of the fireproof polymer–polymer solid-state electrolyte are shown in Figure 1b. The composite SSE is made of a porous bifunctional PI host with Li-ion conductive SPE fillers. The bifunctional host is composed of nonflammable and robust 10- μ m-thick porous polyimide (PI) film with lightweight flame-retardant material decabromodiphenyl ethane (DBDPE), which is not only mechanically strong to prevent potential lithium dendrite penetration but also enables the fireproof ability of SSE. The SPE fillers are composed of PEO/lithium bis(trifluoromethanesulfonylimide) (LiTFSI), ensuing high ionic conductivity of SSEs. The ultrathin and polymer–

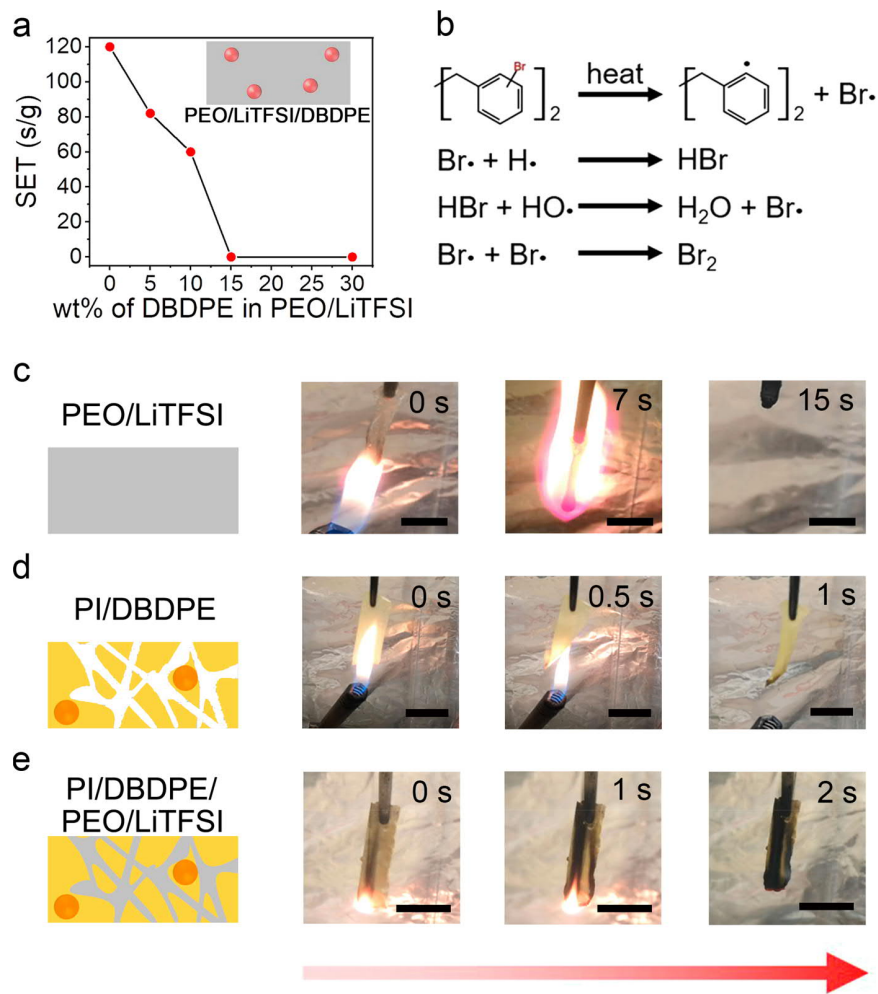


Figure 3. (a) The SET of the PEO/LiTFSI with different weight percentages of DBDPE. (b) The mechanism for the flame retardance effects of DBDPE. Flame tests of (c) PEO/LiTFSI, (d) PI/DBDPE, and (e) PI/DBDPE/PEO/LiTFSI. Scale bars, 1 cm.

polymer nature of the composite electrolyte enables great flexibility, low electrolyte resistance, and potentially high energy density of full batteries. When thermal runaway happens in the battery with PI/DBDPE/PEO/LiTFSI SSE, the flame retardant DBDPE in the nonflammable PI host will effectively suppress the combustion of the flammable PEO/LiTFSI. Figure S2 shows the synthetic procedure of the PI/DBDPE film. We first prepared an intermediate polyamic acid (PAA) solution with DBDPE (see Supporting Information for more details). The solution was then coated onto a glass substrate by doctor blading to produce the PAA/DBDPE film. The dimethylacetamide/ethanol (DMAC/EtOH) solution was used to make the porous PAA/DBDPE film. After drying, the porous PAA/DBDPE film was imidized at 300 °C to yield the final porous PI/DBDPE film. The facial, solution-based process enables the potential scalable production of such host. Figure 1c shows the photo image of the final PI/DBDPE film.

Detailed characterizations of PI/DBDPE film were carried out using scanning electron microscopy (SEM). Figure 2a shows the surface morphology of the PI/DBDPE film on the air-facing side during the doctor blading process. The pores and DBDPE particles were uniformly distributed on the air-facing surface of PI/DBDPE film. The magnified SEM image

of the air-facing surface on PI/DBDPE film shows that the diameter of the pores is around 500 nm. The orange dashed circle represents the DBDPE particle. As shown in Figure S3, the diameter of DBDPE particles ranged from a submicron to a few microns. The surface morphology of the PI/DBDPE film on the glass-facing side is shown in Figure 2b, on which DBDPE particles are less than that on the air-facing side. The pores are well-distributed on the surface facing glass with the pore sizes around 500 nm, similar to that facing air. The cross-section SEM of the typical PI/DBDPE film exhibited excellent uniformity with a constant thickness around 10 μm (Figure 2c). It is noted that, by applying doctor blading with various gap depths, the thickness of the film (10–25 μm) can be easily tuned. The porous structure of PI/DBDPE film was further confirmed by the magnified SEM, where the orange dashed circles represent the DBDPE particles. The nanopores inside the PI/DBDPE film are distributed uniformly, and the sizes are determined to be ~500 nm.

We prepared pure porous PI film with a similar thickness as a comparison. Figure S7 shows SEM characterizations of porous PI film. The surface morphology of the porous PI film on both the air-facing side and glass-facing side shows that the pores are uniformly distributed (Figure S7a,b). The diameter of pores was determined to be ~1 μm and ~500 nm on the air-

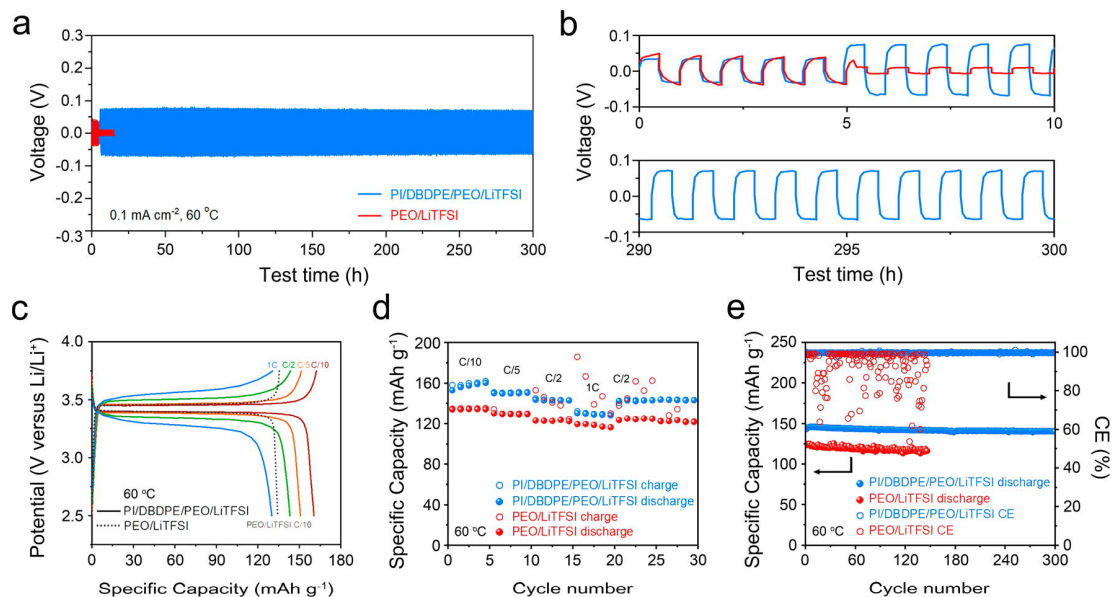


Figure 4. (a) Long-term cycling of symmetrical Li–Li cells with PI/DBDPE/PEO/LiTFSI SSE and PEO/LiTFSI thin-film electrolytes at 60 °C. Each cycle lasts for 1 h. (b) Voltage profile of symmetrical Li–Li cells with PI/DBDPE/PEO/LiTFSI SSE and PEO/LiTFSI thin-film electrolyte from the 0th to the 10th cycles and from the 290th to the 300th cycles. (c) Voltage profile of a Li/PI/DBDPE/PEO/LiTFSI/LFP cell at different charging rates, cycled at 60 °C. The black dashed line represents the Li/PEO/LiTFSI/LFP cell at C/10, cycled at 60 °C. (d) Rate performance of a Li/PEO/LiTFSI/LFP cell and a Li/PI/DBDPE/PEO/LiTFSI/LFP cell, cycled at 60 °C. (e) Cycling performance of Li/PEO/LiTFSI/LFP and Li/PI/DBDPE/PEO/LiTFSI/LFP cells at C/2, cycled at 60 °C.

facing side and glass-facing side, respectively. As shown in the cross-section SEM, the thickness of porous PI film was identified to be 10 μm , similar to that of PI/DBDPE film (Figure S7c). Figure 2d shows the typical FTIR spectra of the PI film and DBDPE particles. Strong characteristic symmetric C=O stretching and C–N stretching signals of PI were identified at $\sim 1719.2\text{ cm}^{-1}$ and $\sim 1372.1\text{ cm}^{-1}$, respectively. Peaks at $\sim 1449.7\text{ cm}^{-1}$ and $\sim 554.4\text{ cm}^{-1}$ of DBDPE were ascribed to strong C=C stretching of a benzene ring and C–Br stretching signals, respectively. All of the peaks match well with the typical PI and DBDPE, which confirms the chemical composition of the synthesized PI, DBDPE, and PI/DBDPE film.

Thermal stability is a critical parameter of a separator. A low melting temperature of a separator can give rise to severe separator shrinkage in the early stage of an internal short circuit, which may accelerate the thermal runaway process. Figure 2e shows the differential scanning calorimetry analysis (DSC) of PI/DBDPE, PI, and PEO/LiTFSI film. No endothermic peak corresponding to polymer melting was observed for the PI/DBDPE and PI film in the whole scanning range, while PEO/LiTFSI exhibited a strong endothermic peak at $\sim 180\text{ °C}$. As such, PI/DBDPE and PI film showed a much higher thermal stability than PEO/LiTFSI. Stress–strain curves of PI/DBDPE, PI, and PEO/LiTFSI film obtained through tensile tests were plotted in Figure 2f. The porous PI/DBDPE film showed a Young’s modulus of 440 MPa, slightly lower than that of pure porous PI film (470 MPa), but almost 4 orders of magnitude higher than that of PEO/LiTFSI (0.1 MPa). In this case, the mechanical strength of the PI/DBDPE film was similar to that of PI film but much larger than that of PEO/LiTFSI.

To quantitatively explore the flame retardant property of DBDPE, we measured the self-extinguishing time (SET) of PEO/LiTFSI electrolytes with different DBDPE concentra-

tions (Figure 3a). The SET was obtained by normalizing the flame combustion time against the electrolyte mass. The pristine PEO/LiTFSI was highly flammable with a SET of $\sim 120\text{ s/g}$. The SET of the PEO/LiTFSI gradually decreased as the DBDPE was added, indicating the flammability of PEO/LiTFSI was reduced as the weight percentage of DBDPE increased. The SET value dropped to zero when the concentration of DBDPE in PEO/LiTFSI increased to 15 wt % (Figure S8a and Video S3). The mechanism for the fireproof property of DBDPE was suggested to be the free-radical scavenging reaction (Figure 3b). DBDPE can degrade to generate Bromo free radicals ($\text{Br}\bullet$) upon heating. The highly reactive radicals $\text{H}\bullet$ and $\text{OH}\bullet$ emitted by the burning electrolyte can be captured by $\text{Br}\bullet$, weakening or terminating combustion chain branching reactions.⁴⁶ Moreover, the gas phase product such as HBr , H_2O , and Br_2 released in a free-radical scavenging reaction limits the heat and mass transfer. These gas products dilute the concentration of oxygen between the heat source and electrolyte, thus retarding the self-sustaining combustion.⁴⁷

The efficiency of DBDPE in suppressing the combustion of PI/DBDPE/PEO/LiTFSI SSE was studied by flame tests. The weight percentage of DBDPE was determined to be 30% in the PI film. PEO/LiTFSI and PI/DBDPE films served as control samples. The PI/DBDPE/PEO/LiTFSI film exhibited an excellent flame retardancy in flame tests. As shown in Figure 3c and Video S4, PEO/LiTFSI without DBDPE caught fire immediately as the lighter approached and then combusted violently. Figure 3d and Video S5 show the flame test of the porous PI/DBDPE film. The PI/DBDPE film twisted because of the extreme heat but did not catch fire. After the pores of the PI/DBDPE film were filled with the flammable PEO/LiTFSI, the ignition and burning of PEO/LiTFSI were effectively suppressed, and the SSE remains intact because of the fireproof material DBDPE in the SSEs (Figure 3e and

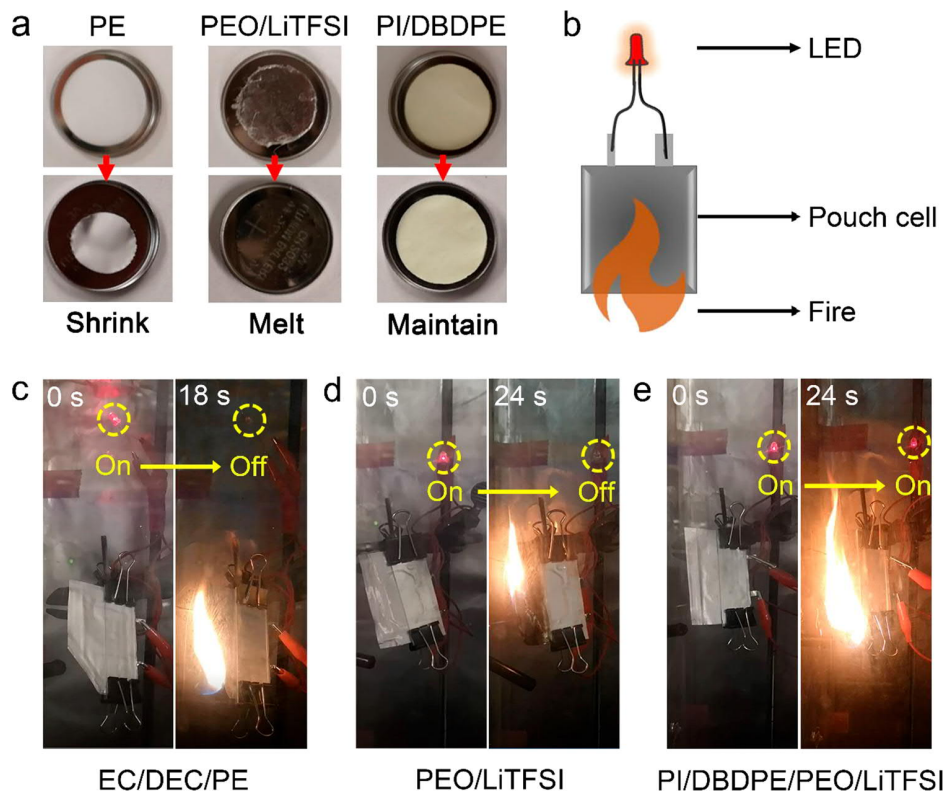


Figure 5. (a) Photo images of PE separator, PEO/LiTFSI, and PI/DBDPE film before/after exposure to thermal shock (150 °C, 0.5 h), respectively. (b) Schematic illustration of the thermal abuse test of the pouch cell battery with LFP as the cathode and LTO as the anode. (c, d, e) Flame abuse test of batteries with (c) EC/DEC/PE, (d) PEO/LiTFSI, and (e) PI/DBDPE/PEO/LiTFSI as the electrolyte, respectively.

Video S6). To further investigate the fireproof property of DBDPE, we took PI and PI/PEO/LiTFSI to flame test as a contrast. The PI film was nonflammable, as shown in Figure S8b and Video S7. However, PI/PEO/LiTFSI easily ignited (Figure S8c and Video S8), indicating the essentiality of DBDPE in suppressing the combustion of SSE.

The cycling test of Li/SSE/Li symmetric cells was carried out to evaluate the mechanical stability of PI/DBDPE/PEO/LiTFSI SSE during the Li plating and stripping process (Figure 4a). The current density was first set to be 0.05 mA cm⁻² at 60 °C to activate the Li/SSE/Li symmetric cells. After the current density was improved to be 0.1 mA cm⁻² in the sixth cycle, a hard short occurred immediately in plain PEO/LiTFSI cells (Figure 4b). However, the PI/DBDPE/PEO/LiTFSI SSE demonstrated a much more stable performance during Li plating and stripping, lasting 300 h at 60 °C. The long, durable performance resulted from the increased modulus of the PI/DBDPE/PEO/LiTFSI SSE, indicating the ability of the proposed high-modulus-matrix structures to prevent dendrite formation.

The electrochemical test of PI/DBDPE/PEO/LiTFSI SSE was conducted at 60 °C in half cells. The cathode and anode of the coin cell were made with LiFePO₄ (LFP) and Li metal, respectively. Control cells were made with the same cathodes and anodes, except for PEO/LiTFSI as the solid-state electrolyte. As shown in Figure 4c, the PI/DBDPE/PEO/LiTFSI cells delivered an excellent rate performance. Voltage profiles at different rates showed clear plateaus at around 3.45 V, which was typical for LFP cathodes. The PI/DBDPE/PEO/LiTFSI cell maintained very low overpotentials of 40 mV at C/10 rates, reflecting the thin nature and thus the low ionic

resistance of PI/DBDPE/PEO/LiTFSI film. In contrast, a relatively large overpotential of 56 mV was observed at C/10 for LFP/PEO/LiTFSI/Li. When cycled at C/10, C/5, C/2, and 1 C, the LFP/PI/DBDPE/PEO/LiTFSI/Li half cell delivered high specific capacities of 163 mAh g⁻¹, 152 mAh g⁻¹, 143 mAh g⁻¹, and 131 mAh g⁻¹, respectively (Figure 4d). However, the specific capacities of LFP/PEO/LiTFSI/Li half cells were only 134 mAh g⁻¹, 129 mAh g⁻¹, 122 mAh g⁻¹, and 115 mAh g⁻¹ when cycling at C/10, C/5, C/2, and 1 C, respectively, much lower than that of the LFP/PI/DBDPE/PEO/LiTFSI/Li cell. These results demonstrated that the rate capability of PI/DBDPE/PEO/LiTFSI SSE was much better compared to PEO/LiTFSI SSE. Figure 4e shows the specific capacity and Coulombic efficiency (CE) of the LFP/PI/DBDPE/PEO/LiTFSI/Li cell and LFP/PEO/LiTFSI/Li cell cycling at the rate of C/2. The LFP/PI/DBDPE/PEO/LiTFSI/Li cell showed stable cycling for more than 300 cycles, whereas the CE of LFP/PEO/LiTFSI/Li cell varied dramatically during cycling. The electrochemical test results showed excellent performance of PI/DBDPE/PEO/LiTFSI SSE for battery operations.

We compared the thermal stability of the PI/DBDPE matrix with PE separator and PEO/LiTFSI (Figure 5a). After exposure to thermal shock conditions (150 °C, 0.5 h), the area of the PE separator shrank to only half as large as that before thermal shock, while PEO/LiTFSI melted. In contrast, no substantial changes in the film dimension and morphology were observed in PI/DBDPE film. To highlight the superior safety of the PI/DBDPE/PEO/LiTFSI cell, a thermal abuse test was conducted. Figure 5b shows the schematic illustration of the pouch cell battery working under flame test conditions.

The cathode and anode materials used for demonstration here were LFP and $\text{Li}_4\text{Ti}_5\text{O}_{12}$ (LTO), respectively, while the only difference in the pouch cells is the electrolytes. As shown in Figure 5c–e, the fully charged liquid electrolyte/polymer separator (ethylene carbonate/diethyl carbonate/polyethylene; EC/DEC/PE) cell, conventional polymer electrolyte (PEO/LiTFSI) cell, and our SSE (PI/DBDPE/PEO/LiTFSI) cell were exposed to flames. The EC/DEC/PE cell and PEO/LiTFSI cell could not light the LED bulbs after ignition for 18 and 24 s, respectively (Video S9 and Video S10). However, the LED bulb operated by the PI/DBDPE/PEO/LiTFSI cell at 24 s was still as bright as that before ignition (Video S11). The remarkable abuse tolerance of the PI/DBDPE/PEO/LiTFSI cell is attributed to the highly thermal-stable PI/DBDPE film, indicating the potential of PI/DBDPE/PEO/LiTFSI SSE to improve the safety of lithium batteries.

In conclusion, fireproof and lightweight SSE with an excellent electrochemical performance can be achieved by utilizing porous PI film with flame-retardant material DBDPE as the host and PEO/LiTFSI as the ionically conducting filler. Compared with conventional PEO/Li salt-based SSEs, the hybrid electrolyte shows an excellent flame-retardant ability. The modulus of the hybrid SSE is 4 orders of magnitude higher than that of the plain PEO/LiTFSI electrolyte, leading to the superior cycling stability of PI/DBDPE/PEO/LiTFSI in Li/SSE/Li cells. Furthermore, the hybrid PI/DBDPE/PEO/LiTFSI solid electrolyte demonstrates a better rate performance and cycling stability than that of plain PEO/LiTFSI in LFP/SSE/Li cells. LFP/PI/DBDPE/PEO/LiTFSI/Li all-solid-state pouch cells also exhibit a high tolerance to abuses such as flame tests. Therefore, the proposed polymer–polymer composite SSE configuration represents a universal and promising route to make high energy density and safe lithium batteries.

■ AUTHOR INFORMATION

Corresponding Author

Yi Cui – Department of Materials Science and Engineering, Stanford University, Stanford, California 94305, United States; SLAC National Accelerator Laboratory, Stanford Institute for Materials and Energy Sciences, Menlo Park, California 94025,

United States; orcid.org/0000-0002-6103-6352;
Email: yicui@stanford.edu

Authors

Yi Cui – Department of Materials Science and Engineering, Stanford University, Stanford, California 94305, United States
Jiayu Wan – Department of Materials Science and Engineering, Stanford University, Stanford, California 94305, United States; orcid.org/0000-0003-4778-1732
Yusheng Ye – Department of Materials Science and Engineering, Stanford University, Stanford, California 94305, United States; orcid.org/0000-0001-9832-2478
Kai Liu – Department of Materials Science and Engineering, Stanford University, Stanford, California 94305, United States; orcid.org/0000-0003-3362-180X
Lien-Yang Chou – Department of Materials Science and Engineering, Stanford University, Stanford, California 94305, United States

Author Contributions

#Y.C., J.W., and Y.Y. contributed equally to this work.

Notes

The authors declare no competing financial interest.

■ ACKNOWLEDGMENTS

The work was supported by the Assistant Secretary for Energy Efficiency and Renewable Energy, Office of Vehicle Technologies of the U.S. Department of Energy under the Battery Materials Research (BMR) program, and Battery 500 Consortium program.

■ REFERENCES

- (1) Armand, M.; Tarascon, J.-M. *Nature* **2008**, *451* (7179), 652–657.
- (2) Lu, J.; Chen, Z.; Ma, Z.; Pan, F.; Curtiss, L. A.; Amine, K. *Nat. Nanotechnol.* **2016**, *11* (12), 1031–1038.
- (3) Sun, Y.; Liu, N.; Cui, Y. *Nat. Energy* **2016**, *1* (7), 1–12.
- (4) Goodenough, J. B.; Park, K. S. *J. Am. Chem. Soc.* **2013**, *135* (4), 1167–1176.
- (5) Guo, Y.; Hu, J.; Wan, L. *Adv. Mater.* **2008**, *20* (15), 2878–2887.
- (6) Dunn, B.; Kamath, H.; Tarascon, J. M. *Science* **2011**, *334* (6058), 928–935.
- (7) Zhang, Q.; Zhang, Z.; Liang, Q.; Gao, F.; Yi, F.; Ma, M.; Liao, Q.; Kang, Z.; Zhang, Y. *Nano Energy* **2019**, *55*, 151–163.
- (8) Liu, Z.; Li, H.; Zhu, M.; Huang, Y.; Tang, Z.; Pei, Z.; Wang, Z.; Shi, Z.; Liu, J.; Huang, Y.; Zhi, C. *Nano Energy* **2018**, *44*, 164–173.
- (9) Lin, D.; Liu, Y.; Cui, Y. *Nat. Nanotechnol.* **2017**, *12* (3), 194–206.
- (10) Xu, W.; Wang, J.; Ding, F.; Chen, X.; Nasybulin, E.; Zhang, Y.; Zhang, J.-G. *Energy Environ. Sci.* **2014**, *7* (2), 513–537.
- (11) Wandt, J.; Marino, C.; Gasteiger, H. A.; Jakes, P.; Eichel, R. A.; Granwehr, J. *Energy Environ. Sci.* **2015**, *8* (4), 1358.
- (12) Braga, M. H.; Grundish, N. S.; Murchison, A. J.; Goodenough, J. B. *Energy Environ. Sci.* **2017**, *10* (1), 331–336.
- (13) Amine, K.; Kanno, R.; Tzeng, Y. *MRS Bull.* **2014**, *39* (5), 395–401.
- (14) Xu, K. *Chem. Rev.* **2014**, *114* (23), 11503–11618.
- (15) Liu, K.; Liu, Y.; Lin, D.; Pei, A.; Cui, Y. *Sci. Adv.* **2018**, *4* (6), No. eaas9820.
- (16) Choi, J. A.; Kim, S. H.; Kim, D. W. *J. Power Sources* **2010**, *195* (18), 6192–6196.

- (17) Chen, S.; Zheng, J.; Yu, L.; Ren, X.; Engelhard, M. H.; Niu, C.; Lee, H.; Xu, W.; Xiao, J.; Liu, J.; Zhang, J. G. *Joule* **2018**, *2* (8), 1548–1558.
- (18) Wu, H.; Zhuo, D.; Kong, D.; Cui, Y. *Nat. Commun.* **2014**, *5*, 5193.
- (19) Chen, Z.; Hsu, P. C.; Lopez, J.; Li, Y.; To, J. W.; Liu, N.; Wang, C.; Andrews, S. C.; Liu, J.; Cui, Y.; Bao, Z. *Nat. Energy* **2016**, *1* (1), 15009.
- (20) Liu, K.; Liu, W.; Qiu, Y.; Kong, B.; Sun, Y.; Chen, Z.; Zhuo, D.; Lin, D.; Cui, Y. *Sci. Adv.* **2017**, *3* (1), No. e1601978.
- (21) Chen, H.; Ling, M.; Hencz, L.; Ling, H. Y.; Li, G.; Lin, Z.; Liu, G.; Zhang, S. *Chem. Rev.* **2018**, *118* (18), 8936–8982.
- (22) Gao, Z.; Sun, H.; Fu, L.; Ye, F.; Zhang, Y.; Luo, W.; Huang, Y. *Adv. Mater.* **2018**, *30* (17), 1705702.
- (23) Fan, X.; Chen, L.; Ji, X.; Deng, T.; Hou, S.; Chen, J.; Zheng, J.; Wang, F.; Jiang, J.; Xu, K.; Wang, C. *Chem.* **2018**, *4* (1), 174–185.
- (24) Bachman, J. C.; Muy, S.; Grimaud, A.; Chang, H. H.; Pour, N.; Lux, S. F.; Paschos, O.; Maglia, F.; Lupart, S.; Lamp, P.; Giordano, L.; Shao-Horn, Y. *Chem. Rev.* **2016**, *116* (1), 140–162.
- (25) Goodenough, J. B.; Singh, P. *J. Electrochem. Soc.* **2015**, *162* (14), A2387–A2392.
- (26) Wan, J.; Xie, J.; Mackanic, D. G.; Burke, W.; Bao, Z.; Cui, Y. *Mater. Today Nano* **2018**, *4*, 1–16.
- (27) Christie, A. M.; Lilley, S. J.; Staunton, E.; Andreev, Y. G.; Bruce, P. G. *Nature* **2005**, *433* (7021), 50–53.
- (28) Zhang, Y.; Wang, Z.; Xiang, H.; Shi, P.; Wang, H. *J. Membr. Sci.* **2016**, *509*, 19–26.
- (29) Kato, Y.; Hori, S.; Saito, T.; Suzuki, K.; Hirayama, M.; Mitsui, A.; Yonemura, M.; Iba, H.; Kanno, R. *Nat. Energy* **2016**, *1* (4), 16030.
- (30) Han, F.; Westover, A. S.; Yue, J.; Fan, X.; Wang, F.; Chi, M.; Leonard, D. N.; Dudney, N. J.; Wang, H.; Wang, C. *Nat. Energy* **2019**, *4* (3), 187.
- (31) Tian, H. K.; Xu, B.; Qi, Y. *J. Power Sources* **2018**, *392*, 79–86.
- (32) Fu, K. K.; Gong, Y.; Hitz, G. T.; McOwen, D. W.; Li, Y.; Xu, S.; Wen, Y.; Zhang, L.; Wang, C.; Pastel, G.; Dai, J.; Liu, B.; Xie, H.; Yao, Y.; Wachsman, E. D.; Hu, L. *Energy Environ. Sci.* **2017**, *10* (7), 1568–1575.
- (33) Manthiram, A.; Yu, X.; Wang, S. *Nat. Rev. Mater.* **2017**, *2* (4), 16103.
- (34) Mindemark, J.; Lacey, M. J.; Bowden, T.; Brandell, D. *Prog. Polym. Sci.* **2018**, *81*, 114–143.
- (35) Miller, T. F., III; Wang, Z. G.; Coates, G. W.; Balsara, N. P. *Acc. Chem. Res.* **2017**, *50* (3), 590–593.
- (36) Wright, P. V. *Br. Polym. J.* **1975**, *7* (5), 319–327.
- (37) Harry, K. J.; Hallinan, D. T.; Parkinson, D. Y.; MacDowell, A. A.; Balsara, N. P. *Nat. Mater.* **2014**, *13* (1), 69–73.
- (38) Stone, G. M.; Mullin, S. A.; Teran, A. A.; Hallinan, D. T.; Minor, A. M.; Hexemer, A.; Balsara, N. P. *J. Electrochem. Soc.* **2012**, *159* (3), A222–A227.
- (39) Lin, D.; Liu, W.; Liu, Y.; Lee, H. R.; Hsu, P. C.; Liu, K.; Cui, Y. *Nano Lett.* **2016**, *16* (1), 459–465.
- (40) Sheng, O.; Jin, C.; Luo, J.; Yuan, H.; Huang, H.; Gan, Y.; Zhang, J.; Xia, Y.; Liang, C.; Zhang, W.; Tao, X. *Nano Lett.* **2018**, *18* (5), 3104–3112.
- (41) Xue, Z.; He, D.; Xie, X. *J. Mater. Chem. A* **2015**, *3* (38), 19218–19253.
- (42) Lopez, J.; Mackanic, D. G.; Cui, Y.; Bao, Z. *Nat. Rev. Mater.* **2019**, *4* (5), 312–330.
- (43) Lin, D.; Yuen, P. Y.; Liu, Y.; Liu, W.; Liu, N.; Dauskardt, R. H.; Cui, Y. *Adv. Mater.* **2018**, *30* (32), 1802661.
- (44) Zhang, J.; Zhao, J.; Yue, L.; Wang, Q.; Chai, J.; Liu, Z.; Zhou, X.; Li, H.; Guo, Y.; Cui, G.; Chen, L. *Adv. Energy Mater.* **2015**, *5* (24), 1501082.
- (45) Wan, J.; Xie, J.; Kong, X.; Liu, Z.; Liu, K.; Shi, F.; Pei, A.; Chen, H.; Chen, W.; Chen, J.; Zhang, X.; Zong, L.; Wang, J.; Chen, L. Q.; Qin, J.; Cui, Y. *Nat. Nanotechnol.* **2019**, *14* (1), 705–711.
- (46) Zuo, J. D.; Li, R. X.; Feng, S. H.; Liu, G. Y.; Zhao, J. Q. *J. Cent. South Univ. Technol.* **2008**, *15* (1), 64–68.
- (47) Ye, L.; Meng, X. Y.; Liu, X. M.; Tang, J. H.; Li, Z. M. *J. Appl. Polym. Sci.* **2009**, *111* (5), 2372–2380.